SOLID STATE PHYSICS

MAGNON AND PHONON EXCITATIONS IN NANOSIZED NiO

N. Mironova-Ulmane [1], A. Kuzmin [1], I. Sildos [2], L. Puust [2], J. Grabis [3]

[1] Institute of Solid State Physics, University of Latvia,
8 Kengaraga Str., Riga, LV-1063, LATVIA
E-mail: nina@cfi.lu.lv

[2] Institute of Physics, University of Tartu, 1 Ostwaldi, 50411 Tartu, ESTONIA

[3] Riga Technical University, Institute of Inorganic Chemistry,
3/7 P. Valdena Str., LV-1048, Riga, LATVIA

Single-crystal, microcrystalline and nanocrystalline nickel oxides (NiO) have been studied by Raman spectroscopy. A new band at ~200 cm^{-1} and TO-LO splitting of the band at 350–650 cm^{-1} have been found in the spectra of single-crystals NiO(100), NiO(110) and NiO(111). The Raman spectra of microcrystalline (1500 nm) and nanocrystalline (13–100 nm) NiO resemble those of the single crystals. They all contain the two-magnon band at 1500 cm^{-1}, indicating that the oxides remain at room temperature in the antiferromagnetic phase. Besides, a new sharp Raman band has been observed at 500 cm^{-1} in nanocrystalline NiO. Its temperature dependence suggests the magnetic origin of the band, possibly associated with the one-phonon–one-magnon excitation at the Brillouin zone centre.

Keywords: *lattice dynamics, magnons, nickel oxide, nanoparticles, Raman spectroscopy*

1. INTRODUCTION

Nickel oxide (NiO) is a versatile compound, which finds numerous applications in rechargeable batteries [1], smart windows [2], catalysis [3], sensors [4], gamma radiation detectors [5], resistive memories [6] and magnetoresistive devices [7].

Bulk NiO is a highly correlated material, which features a Mott insulating character and a type-II easy-plane antiferromagnetic (AFM) ordering. Therefore, the understanding of its electronic structure and bonding was a challenging theoretical task for decades. In the paramagnetic phase above the Néel temperature T_N = 523 K, NiO has a centrosymmetric cubic rock-salt crystal structure (space group No. 225, *Fm-3m*) with nickel ions located at the centres of regular NiO_6 octahedra [8]. The ferromagnetic ordering of spins of Ni^{2+} ions occurs below T_N in {111} sheets, with adjacent sheets having antiparallel spins [9], [10]. Such spin ordering leads

to a magnetostriction effect, causing a week cubic-to-rhombohedral distortion (space group No. 166, *R-3m*) of the NiO structure [8], [11]–[15], The distortion is accompanied by splitting (about 10–40 cm^{-1} at 300 K) of the zone centre transverse optical (TO) mode [16]–[18]. The magnetic structure of NiO nanoparticles differs from that of the bulk because of the finite-size effects and the presence of defects [19]. A complex magnetic structure composed of as many as up to eight-sublattice spin configurations was proposed for NiO nanoparticles [20]–[22] in contrast to the single-crystal NiO, having the two-sublattice magnetic structure [8]. Apart from the antiferromagnetically ordered core, magnetically-disordered uncompensated spins exist at the surface of NiO nanoparticles [23]–[29], leading to a super-paramagnetic behaviour [30].

Neutron diffraction studies of plate-shaped NiO nanoparticles with a thickness of ~2 nm indicated a reduction of the Néel temperature by ~60 K [31]. Comparison of X-ray and neutron diffraction data also evidenced the identity of the magnetic and crystallographic correlation lengths, suggesting that each NiO nanoparticle consists of a single magnetic domain [31]. Finally, a significant lattice expansion and a crossover in magnetic properties occur in NiO nanoparticles when their size decreases below 30 nm [32]. An increase of the lattice parameter in NiO nanoparticles upon a decrease of their sizes was observed below 20 nm in [33] and below 12 nm in [34].

The magnetic ordering and lattice dynamics of microcrystalline and single-crystalline NiO were studied by Raman spectroscopy in [35]–[42]. The Raman spectrum of bulk NiO at room temperature consists of several bands due to second-order phonon scattering (2TO band at ~730 cm^{-1}, TO+LO band at ~906 cm^{-1} and 2LO band at ~1090 cm^{-1}) and two-magnon band (at ~1500 cm^{-1}) [35]–[38], [40], [42]. The main difference between green (stoichiometric) and black (defect-reach) bulk NiO was a dramatic increase in the strength of the one-phonon LO mode at 550-560 cm^{-1} in the black NiO [35]. The origin of phonon bands was interpreted theoretically using the rigid-ion [43]–[46], shell [47], and first principles [42], [48] models. It was also proposed that some nonmagnetic properties of NiO as zone-centre optical phonon frequencies and Born effective charge tensor are substantially noncubic below the Néel temperature, even assuming the ideal rock-salt structure of the oxide [49].

The influence of finite-size and preparation conditions on the vibrational properties and magnetic ordering in nanocrystaline NiO was studied by Raman spectroscopy in [28], [34], [50]–[54]. The phonon-related bands in the Raman spectra of large green nanocrystals (100–1500 nm), produced by radio-frequency plasma technique, are close to those in the bulk [50]. However, the enhancement of the band at 500 cm^{-1} was found in small black nanocrystals (13–23 nm) produced by precipitation method, and the band was associated with the phonon-magnon coupling at the nanoparticle surface or with the presence of defects [51].

Small NiO nanoparticles (3.5–12.4 nm) were produced in [34] by a decomposition of nickel acetate at different temperatures. Their Raman spectra resemble those in [50]. Still, they do not show any peak related to the magnon excitation at 1500 cm^{-1} as well as any enhancement of 500 cm^{-1} band [34]. A contribution from surface modes to the broadening of LO and 2LO bands was also

proposed in [34].

The sol-gel method followed by annealing in air was employed in [52] to synthesize NiO nanoparticles in the range of 16.6–54 nm. The Raman spectrum of the smallest particles (16.6 nm) was dominated by the one-phonon (TO and LO) scattering; however, the two-phonon and two-magnon bands became also visible upon increasing particle size. Close results were obtained for nanosized NiO powders prepared by ball milling process under different milling speeds in [53]. In the latter case, a decrease of the crystallite size from 43 nm to 10.5 nm led to a reduction of the two-phonon band intensity, whereas the two-magnon band was not detected in all milled samples [53].

Nanocrystalline NiO (~26–36 nm) with filamentary morphology and large amount of nickel vacancies was produced by the template-based method using the cellulose template [54]. As a result, the one-phonon Raman bands (TO at 400 cm^{-1} and LO at 500 cm^{-1}) were strongly enhanced compared with the two-phonon band at ~1090 cm^{-1}. In addition, the presence of the intense two-magnon band at ~1500 cm^{-1} indicated the existence of the antiferromagnetic order at room temperature. Note that similar Raman spectra were observed for NiO nanoparticles in the range of 6.1–79.8 nm prepared by the precipitation method [28], except that the two-magnon peak disappeared for the 6.1 nm sample.

In the present study, we have employed the temperature-dependent Raman spectroscopy to probe the phonon and magnon dynamics in single-crystal NiO with different orientations (100), (110), (111) and in NiO nanoparticles. Two new bands at ~200 cm^{-1} and ~500 cm^{-1} have been evidenced, and their origin will be discussed.

2. EXPERIMENTAL STUDY

Nanocrystalline NiO powders were produced by two methods. A precipitation method, based on a reaction of aqueous solutions of $Ni(NO_3)_2 \cdot 6H_2O$ and NaOH with subsequent annealing in air at several temperatures up to $T_{an} = 450 °C$, was employed to produce the smallest black NiO nanoparticles. Their average sizes were estimated from the BET specific surface area measurements and were equal to about 13 nm for powders annealed at $T_{an} = 250 °C$ and 300 °C, 17 nm at $T_{an} = 350 °C$, and 23 nm at $T_{an} = 450 °C$. In the second method, green NiO particles with larger size of 100 nm and 1500 nm were prepared by evaporation of coarse grained commercially available NiO (99.9 %) powder with the particle size in the range of 20–40 μm in the radio-frequency plasma [50].

Three green coloured single-crystals NiO(100), NiO(110) and NiO(111) were grown on top of MgO(100), MgO(110) and MgO(111) single-crystal substrates, respectively, using the method of chemical transport reaction [55], [56].

The Raman spectra were measured with large signal/noise ratio and particular attention to exclude any unintentional sample overheating by the laser light. High-temperature (20–290 °C) Raman experiments were conducted using a confocal microscope with spectrometer Nanofinder-S (SOLAR-TII, Ltd.). The measurements were performed through 20× optical objective. The Raman spectra were excited by a solid-state DPSS 532 nm laser (max cw power 150 mW). The Peltier-cooled back-

thinned CCD camera was used as a detector. The elastic laser light component was eliminated by the edge filter (Semrock RazorEdge, LP03-532RE-25). The sample temperature was controlled by self-made optical furnace. Room temperature Raman spectra were also measured through 50× microscope objective using Renishaw inVia micro-Raman spectrometer equipped with argon laser (514.5 nm, max cw power 10 mW). The spectral signal was dispersed by the 2400 grooves/mm grating onto Peltier-cooled (-60 °C) CCD detector.
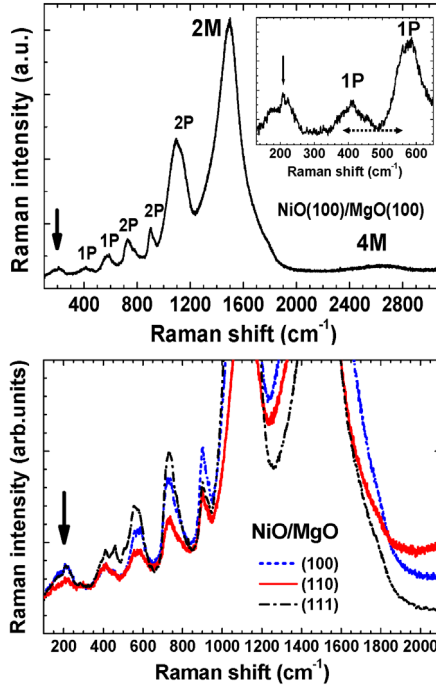

Fig. 1. Room temperature Raman spectra of green single-crystals NiO(100), NiO(110) and NiO(111). Enlarged low-frequency range is shown in the inset. The arrows indicate previously unclassified band at ~200 cm⁻¹.

3. RESULTS AND DISCUSSION

Room temperature Raman spectrum of single-crystal NiO(100) consists of several bands above 300 cm⁻¹ (Fig. 1). According to the previous assignment in [35], [36] based on the cubic NiO structure, the first five bands are due to the phonon scattering: one-phonon (1P) TO and LO modes (at ~400 cm⁻¹ and ~580 cm⁻¹, respectively), two-phonon (2P) 2TO modes (at ~730 cm⁻¹), TO+LO (at ~906 cm⁻¹) and 2LO (at ~1090 cm⁻¹) modes. The strongest band at 1500 cm⁻¹ is due to the two-magnon (2M) scattering [35], [37]. Note that the band at ~2640 cm⁻¹ corresponds to the four-magnon (4M) scattering [36]. At 1.5 K, the 4M band is located at ~2800 cm⁻¹ and has a pronounced shape [36], but it broadens and shifts to lower frequencies as temperature increases. Two differences are observed between the Raman spectra of single-crystals NiO in Fig. 1 and those measured in [35], [38], [40]: the one-phonon band at ~350–650 cm⁻¹ is split into two (TO and LO) bands located at ~400 and ~580 cm⁻¹, and a new band appears at ~200 cm⁻¹. Note that the TO-LO splitting

of the one-phonon band has also been observed in the recent study [42]. We attribute the origin of the band at 200 cm^{-1} to the zone-boundary phonon mode [57].

Temperature dependence of the Raman spectra for two stoichiometric single-crystals NiO(100) and NiO(111) is shown in Fig. 2. The main visible effect is related to a decrease of intensity and a displacement to lower frequencies of the two-magnon band at ~1500 cm^{-1}, when the sample temperature is approaching the Néel temperature. The band at 200 cm^{-1} as well as the two (TO and LO) bands at 400 and 580 cm^{-1} remain well visible at all temperatures. One can also see that the TO band at 400 cm^{-1} exhibits splitting below the Néel temperature due to the magnetic-order induced phonon anisotropy [16], [18], which appears at room temperature as a shoulder or a narrow peak located at 460 cm^{-1} in the Raman spectrum of single-crystal NiO(111).

Room temperature Raman spectra of nanocrystalline (13–23 nm) NiO (Fig. 3), produced at different annealing temperatures in the range of 250–450 °C, are rather similar to that of the bulk material except for a narrow strong band around 500 cm^{-1}. The phonon-related Raman bands (1P and 2P in Fig. 3) in nanocrystalline NiO are close to those in single-crystals: they consist of a small band (1P) at ~200 cm^{-1}, a wide one-phonon (1P) band at ~300-600 cm^{-1} and two-phonon (2P) bands at ~730 cm^{-1}, ~900 cm^{-1} and ~1100 cm^{-1}. The intensity of the one-phonon (1P) bands relative to that of the 2P bands is higher in nanopowders due to the presence of defects or surface effect, while the three two-phonon (2P) bands appear to be more broadened than in single-crystal NiO. Similar behaviour of the phonon-related Raman bands in nanopowders was reported in [58]. The two-magnon (2M) band located at ~1500 cm^{-1} has in nanopowders smaller intensity compared to the two-phonon band at ~1100 cm^{-1} since the size effect limits the long-range magnetic order.
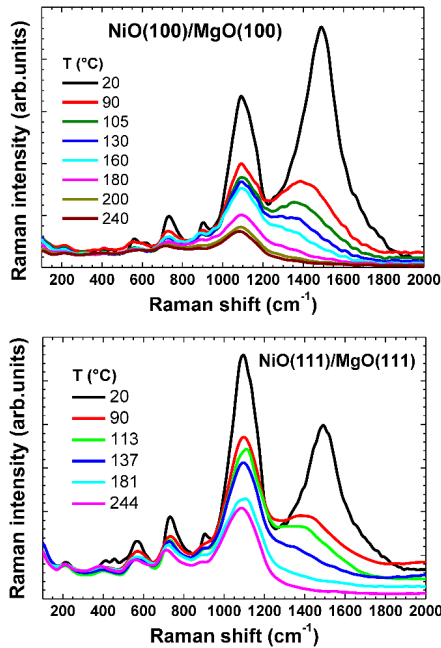

Fig. 2. Temperature dependent Raman spectra of green single-crystals NiO(100)/MgO(100) and NiO(111)/MgO(111) measured in the temperature range between 20 °C and 250 °C.
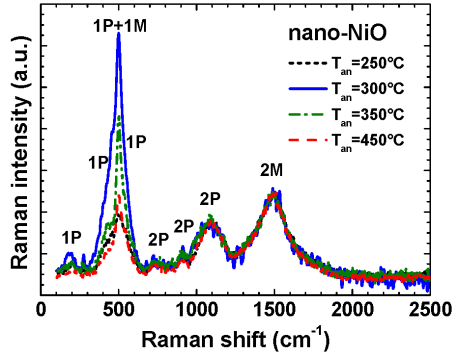
Fig. 3. Room temperature Raman spectra of nanocrystalline (13–23 nm) NiO powders produced by annealing at different temperatures. Laser excitation power P_{ex} = 0.1 mW.
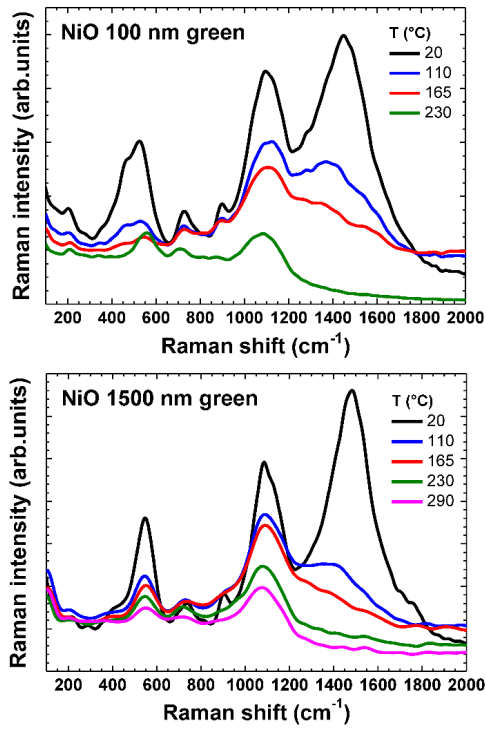

Fig. 4. Temperature dependent Raman spectra of nanocrystalline (100 nm) and microcrystalline (1500 nm) NiO powders.

Temperature dependence of the Raman scattering in nanocrystalline (100 nm) and microcrystalline (1500 nm) NiO powders is shown in Fig. 4 and is close to that in single-crystal NiO in Fig. 2. The most intriguing fact is the behaviour of the band at ~400–600 cm^{-1}. Its intensity at room temperature is rather high and correlates with the intensity of the two-magnon band at 1500 cm^{-1}, which decreases upon heating until it disappears approaching the Néel temperature. Therefore, one can suspect that the band at ~400–600 cm^{-1} has some magnon-related origin.

Heating of the sample can be achieved not only in an optical furnace, but

also when the laser power is changed. In this case, the precise value of temperature is not known but for NiO can be roughly estimated from the intensity and position of the two-magnon band at ~1500 cm^{-1}. Such an experiment was conducted for nanocrystalline (17 nm) NiO powder. The obtained Raman spectra are shown in Fig. 5. We started at the low laser power of P_{ex} = 0.1 mW at the sample with no sample heating as is evidenced from the large intensity of the two-magnon band. Upon increasing the laser power ten times up to P_{ex} = 1 mW at the sample, the intensity of the two-magnon band decreases, and its position shifts down to ~1400 cm^{-1}. The shift of the two-magnon band contributes to a change in the background under other bands, thus making problematic their proper normalization [42]. At the same time, the position of the phonon-related bands remains nearly unchanged upon laser heating. Further increase of the laser power to P_{ex} = 5 mW at the sample leads to a complete disappearance of the two-magnon band, suggesting heating above the Néel temperature and, thus, destruction of the magnetic ordering. Note that when the laser power is decreased back to P_{ex} = 0.1 mW, the shape of the Raman spectrum is completely restored to the original one, indicating the reversibility of the transition and the absence of any sample damage.
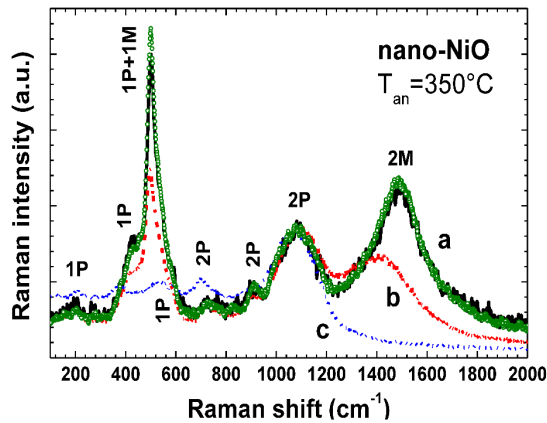

Fig. 5. The Raman spectra of nanocrystalline (17 nm) NiO powder (annealed at 350 °C) measured at different laser excitation powers: (a) P_{ex} = 0.1 mW (solid line – the first measurement; open circles – the final measurement); (b) P_{ex} = 1 mW; (c) P_{ex} = 5 mW. The phonon and magnon related bands are indicated.

Note that the Raman spectrum of nanocrystalline (17 nm) NiO powder contains a narrow band at 500 cm^{-1}, which is temperature dependent and correlates well with the two-magnon band (Fig. 5). This band also demonstrates the dependence on the size of nanocrystallites in Fig. 3. Therefore, we tentatively attribute the origin of this band to scattering by two particles: one-phonon (~440 cm^{-1}) and one-magnon (~40 cm^{-1}) excited simultaneously at the Brillouin zone centre due to the strong phonon-magnon coupling occurring at the nanoparticle surface or defects. Upon a decrease in the nanoparticle size, the intensity of the band at 500 cm^{-1} changes as a result of the competition between two processes: (i) an increase in the surface-to-bulk ratio and defect concentration, and (ii) a destruction of the long-range magnetic ordering [59].

4. CONCLUSIONS

Raman scattering by phonons and magnons has been studied in single-crystal, microcrystalline (1500 nm) and nanocrystalline (13–100 nm) NiO powders. The Raman spectra of nanocrystalline NiO have been found to be qualitatively similar to those of single-crystal, including the two-magnon band at 1500 cm^{-1}, indicating that the nanopowders remain at room temperature in antiferromagnetic phase.

A weak but clearly visible new band at ~200 cm^{-1} has been found in the Raman spectra of all samples and attributed to the zone-boundary phonon mode [57]. TO-LO splitting of the phonon band at 350–650 cm^{-1} has been observed in single-crystal NiO. Moreover, the TO band at 400 cm^{-1} is split below the Néel temperature due to the magnetic-ordering induced phonon anisotropy [16], [18]. This effect appears at room temperature as a shoulder or a narrow peak located at 460 cm^{-1} in the Raman spectrum of single-crystal NiO(111). Finally, a sharp intense Raman band has been observed at 500 cm^{-1} in smallest (~13–17 nm) black nanocrystalline NiO powders. The band is located on top of one-phonon bands, and its temperature dependence correlates with that of the two-magnon band at 1500 cm^{-1}, thus suggesting the magnetic origin of the band, possibly associated with the one-phonon–one-magnon excitation at the Brillouin zone centre. The traces of this band have also been detected in microcrystalline NiO powder.

REFERENCES

1. Lee, D. U., Fu, J., Park, M. G., Liu, H., Ghorbani Kashkooli, A., & Chen, Z. (2016). Self-assembled NiO/Ni(OH)$_2$ nanoflakes as active material for high-power and high-energy hybrid rechargeable battery. *Nano Lett.*, *16*, 1794–1802. DOI: 10.1021/acs.nanolett.5b04788

2. Browne, M., Nolan, H., Berner, N., Duesberg, G., Colavita, P., & Lyons, M. (2016). Electrochromic nickel oxide films for smart window applications. *Int. J. Electrochem. Sci.*, *11*, 6636–6647. DOI: 10.20964/2016.08.38

3. Lee, S. G., Lee, S., & Lee, H. I. (2001). Photocatalytic production of hydrogen from aqueous solution containing CN$^-$ as a hole scavenger. *Appl. Catal. A*, 207, 173–181. DOI: 10.1016/S0926-860X(00)00671-2

4. Ando, M., Zehetner, J., Kobayashi, T., & Haruta, M. (1996). Large optical CO sensitivity of NO^2-pretreated Au-NiO composite films. *Sens. Actuators B*, *36*, 513–516. DOI: 10.1016/S0925-4005(97)80121-9

5. Múčka, V., & Baburek, E. (1998). Catalytic properties of nickel-yttrium mixed oxides and the influence of ionizing radiation. *Rad. Phys. Chem.*, *53*, 483–489. DOI: 10.1016/S0969-806X(98)00216-3

6. Lee, C. B., B. S. Kang, B. S., Benayad, A., Lee, M. J., Ahn, S.-E., Kim, K. H., … & Yoo, I. K. (2008). Effects of metal electrodes on the resistive memory switching property of NiO thin films. *Appl. Phys. Lett.*, *93*, 042115. DOI: 10.1063/1.2967194

7. Tsymbal, E. Y., & Pettifor, D. G. (2001). Perspectives of giant magnetoresistance. *Solid State Phys.*, *56*, 113–237. DOI: 10.1016/S0081-1947(01)80019-9

8. Roth, W. L. (1958). Magnetic structures of MnO, FeO, CoO, and NiO. P*hys. Rev.*, *110*, 1333–1341. DOI: 10.1103/PhysRev.110.1333

9. Hutchings, M. T., & Samuelsen, E. J. (1972). Measurement of spin-wave dispersion in NiO by inelastic neutron scattering and its relation to magnetic properties. *Phys. Rev. B*, *6*, 3447–3461. DOI: 10.1103/PhysRevB.6.3447

10. Hillebrecht, F. U., Ohldag, H., Weber, N. B., Bethke, C., Mick, U., Weiss, M., & Bahrdt, J. (2001). Magnetic moments at the surface of antiferromagnetic NiO(100). *Phys. Rev. Lett.*, *86*, 3419–3422. DOI: 10.1103/PhysRevLett.86.3419

11. Rooksby, H. P. (1948). A note on the structure of nickel oxide at subnormal and elevated temperatures. *Acta Crystallogr.*, *1*, 226. DOI: 10.1107/S0365110X48000612

12. Slack, G. A. (1960). Crystallography and domain walls in antiferromagnetic NiO crystals, *J. Appl. Phys.*, *31*, 1571–1582. DOI: 10.1063/1.1735895

13. Massarotti, V., Capsoni, D., Berbenni, V., Riccardi, R., Marini, A., & Antolini, E. (1991). Structural characterization of nickel oxide. *Z. Naturforsch. A*, *46*, 503–512. DOI: 10.1515/zna-1991-0606

14. Rodic, D., Spasojevic, V., Kusigerski, V., Tellgren, R., & Rundlof, H. (2000). Magnetic ordering in polycrystalline $Ni_xZn_{1-x}O$ solid solutions. *Phys. Status Solidi B*, *218*, 527–536. DOI: 10.1002/1521-3951(200004)218:2<527::AID-PSSB527>3.0.CO;2- I

15. Balagurov, A. M., Bobrikov, I. A., Sumnikov, S. V., Yushankhai, V. Y., & Mironova-Ulmane, N. (2016). Magnetostructural phase transitions in NiO and MnO: neutron diffraction data. *JETP Lett.*, *104*, 88–93. DOI: 10.1134/S0021364016140071

16. Chung, E. M. L., Paul, D. M., Balakrishnan, G., Lees, M. R., Ivanov, A., & Yethiraj, M. (2003). Role of electronic correlations on the phonon modes of MnO and NiO. *Phys. Rev. B*, *68*, 140406. DOI: 10.1103/PhysRevB.68.140406

17. Luo, W., Zhang, P., & Cohen, M. L. (2007). Splitting of the zone-center phonon in MnO and NiO. *Solid State Commun.*, *142*, 504–508. DOI: 10.1016/j.ssc.2007.03.047

18. Kant, C., Mayr, F., Rudolf, T., Schmidt, M., Schrettle, F., Deisenhofer, J., & Loidl, A. (2009). Spin-phonon coupling in highly correlated transition-metal monoxides. *Eur. Phys. J. Special Topics*, *180*, 43–59. DOI: 10.1140/epjst/e2010-01211-6

19. Mørup, S., Madsen, D. E., Frandsen, C., Bahl, C. R. H., & Hansen, M. F. (2007). Experimental and theoretical studies of nanoparticles of antiferromagnetic materials. *J. Phys.: Condens. Matter*, *19*, 213202. DOI: 10.1088/0953-8984/19/21/213202

20. Nakahigashi, K., Fukuoka, N., & Shimomura, Y. (1975). Crystal structure of antiferromagnetic NiO determined by X-ray topography. *J. Phys. Soc. Jpn.*, *38*, 1634–1640. DOI: 10.1143/JPSJ.38.1634

21. Kodama, R. H., Makhlouf, S. A., & Berkowitz, A. E. (1997). Finite size effects in antiferromagnetic NiO nanoparticles. *Phys. Rev. Lett.*, *79*, 1393–1396. DOI: 10.1103/ PhysRevLett.79.139

22. Kodama, R. H., & Berkowitz, A. E. (1999). Atomic-scale magnetic modelling of oxide nanoparticles. *Phys. Rev. B*, *59*, 6321–6336. DOI: 10.1103/PhysRevB.59.6321.

23. Tiwari, S. D., & Rajeev, K. P. (2006). Magnetic properties of NiO nanoparticles, *Thin Solid Films*, *505*, 113–117. DOI: 10.1016/j.tsf.2005.10.019

24. Mandal, S., Banerjee, S., & Menon, K. S. R. (2009). Core-shell model of the vacancy concentration and magnetic behavior for antiferromagnetic nanoparticle. *Phys. Rev. B*, *80*, 214420. DOI: 10.1103/PhysRevB.80.214420

25. Mandal, S., Menon, K. S. R., Mahatha, S. K., & Banerjee, S. (2011). Finite size versus surface effects on magnetic properties of antiferromagnetic particles. *Appl. Phys. Lett.*, *99*, 232507. DOI: 10.1063/1.3668091

26. Cooper, J. F. K., Ionescu, A., Langford, R. M., Ziebeck, K. R. A., Barnes, C. H. W., Gruar, R., … & Ouladdiaf, B. (2013). Core/shell magnetism in NiO nanoparticles. *J. Appl. Phys.*, *114*, 083906. DOI: 10.1063/1.4819807

27. Balagurov, A. M., Bobrikov, I. A., Grabis, J., Jakovlevs, D., Kuzmin, A., Maiorov, M., & Mironova-Ulmane, N. (2013). Neutron scattering study of structural and magnetic size effects in NiO. *IOP Conf. Ser.: Mater. Sci. Eng.*, *49*, 012021. DOI: 10.1088/1757-899X/49/1/012021

28. Yang, Z., Gao, D., Tao, K., Zhang, J., Shi, Z., Xu, Q., Shi, S., & Xue, D. (2014). A series of unexpected ferromagnetic behaviors based on the surface-vacancy state: an insight into NiO nanoparticles with a core-shell structure. *RSC Adv.*, *4*, 46133–46140. DOI: 10.1039/C4RA06472K

29. Balagurov, A. M., Bobrikov, I. A., Sumnikov, S. V., Yushankhai, V. Y., Grabis, J., Kuzmin, A., … & Sildos, I. (2016). Neutron diffraction study of microstructural and magnetic effects in fine particle NiO powders. *Phys. Status Solidi B*, *253*, 1529–1536. DOI: 10.1002/pssb.201552680

30. Richardson, J. T., Yiagas, D. I., Turk, B., Forster, K., & Twigg, M. V. (1991). Origin of superparamagnetism in nickel oxide. *J. Appl. Phys.*, *70*, 6977–6982. DOI: 10.1063/1.349826

31. Klausen, S. N., Lindgärd, P. A., Lefmann, K., Bødker, F., & Mørup, S. (2002). Temperature dependence of the magnetization of disc shaped NiO nanoparticles. *Phys. Status Solidi A*, *189*, 1039–1042. DOI: 10.1002/1521- 396X(200202)189:3<1039::AID-PSSA1039>3.0.CO;2-A

32. Li, L., Chen, L., Qihe, R., & Li, G. (2006). Magnetic crossover of NiO nanocrystals at room temperature. *Appl. Phys. Lett.*, *89*, 134102. DOI: 10.1063/1.2357562

33. Makhlouf, S. A., Kassem, M. A., & Abdel-Rahim, M. A. (2009). Particle size-dependent electrical properties of nanocrystalline NiO. *J. Mater. Sci.*, *44*, 3438–3444. DOI: 10.1007/s10853-009-3457-0

34. Duan, W. J., Lu, S. H., Wu, Z. L., & Wang, Y. S. (2012). Size effects on properties of NiO nanoparticles grown in alkalisalts. *J. Phys. Chem. C*, *116*, 26043–26051. DOI: 10.1021/jp308073c

35. Dietz, R. E., Parisot, G. I., & Meixner, A. E. (1971). Infrared absorption and Raman scattering by two-magnon processes in NiO. *Phys. Rev. B*, *4*, 2302–2310. DOI: 10.1103/PhysRevB.4.2302

36. Dietz, R. E., Brinkman, W. F., Meixner, A. E., & Guggenheim, H. J. (1971). Raman scattering by four magnons in NiO and $KNiF_3$. *Phys. Rev. Lett.*, *27*, 814–817. DOI: 10.1103/PhysRevLett.27.814

37. Lockwood, D. J., Cottam, M. G., & Baskey, J. H. (1992). One- and two-magnon excitations in NiO. *J. Magn. Magn. Mater.*, *104*, 1053–1054. DOI: 10.1016/0304-8853(92)90486-8

38. Pressl, M., Mayer, M., Knoll, P., Lo, S., Hohenester, U., & Holzinger-Schweiger, E. (1996). Magnetic Raman scattering in undoped and doped antiferromagnets. *J. Raman Spectroscopy*, *27*, 343–349. DOI: 10.1002/(SICI)1097-4555(199603)27:3/4<343::AID-JRS956>3.0.CO;2-S

39. Grimsditch, M., McNeil, L. E., & Lockwood, D. J. (1998). Unexpected behavior of the antiferromagnetic mode of NiO. *Phys. Rev. B*, *58*, 14462–14466. DOI: 10.1103/PhysRevB.58.14462

40. Cazzanelli, E., Kuzmin, A., Mariotto, G., & Mironova-Ulmane, N. (2003). Study of vibrational and magnetic excitations in $Ni_cMg_{1-c}O$ solid solutions by Raman spectroscopy. *J. Phys.: Condensed Matter*, *15*, 2045. DOI: 10.1088/0953-8984/15/12/321

41. Cazzanelli, E., Kuzmin, A., Mironova-Ulmane, N., & Mariotto, G. (2005). Behavior of one-magnon frequency in antiferromagnetic $Ni_cMg_{1-c}O$ solid solutions. *Phys. Rev. B*, *71*, 134415. DOI: 10.1103/PhysRevB.71.134415

42. Aytan, E., Debnath, B., Kargar, F., Barlas, Y., Lacerda, M. M., Li, J. X., … & Balandin, A. A. (2017). Spin-phonon coupling in antiferromagnetic nickel oxide. *Appl. Phys. Lett.*, *111*, 252402. DOI: 10.1063/1.5009598

43. Haywood, B. C. G., & Collins, M. F. (1969). Lattice dynamics of MnO. *J. Phys. C: Solid State Phys.*, *2*, 46. DOI: 10.1088/0022-3719/2/1/306

44. Haywood, B. C. G., & Collins, M. F. (1971). Optical phonons in MnO. *J. Phys. C: Solid State Phys.*, *4*, 1299. DOI: 10.1088/0022-3719/4/11/005

45. Upadhyaya, K. S., & Singh, R. K. (1974). Shell model lattice dynamics of transition metal oxides. *J. Phys. Chem. Solids*, *35*, 1175–1179. DOI: 10.1016/S0022- 3697(74)80137-X

46. Reichardt, W., Wagner, V., & Kress, W. (1975). Lattice dynamics of NiO. *J. Phys. C: Solid State Phys.*, *8*, 3955. DOI: 10.1088/0022-3719/8/23/009

47. Coy, R. A., Tompson, C. W., & Gürmen, E. (1976). Phonon dispersion in NiO. *Solid State Commun.*, *18*, 845–847. DOI: 10.1016/0038-1098(76)90220-9

48. Savrasov, S. Y., & Kotliar, G. (2003). Linear response calculations of lattice dynamics in strongly correlated systems. *Phys. Rev. Lett.*, *90*, 056401. DOI: 10.1103/ PhysRevLett.90.056401

49. Massidda, S., Posternak, M., Baldereschi, A., & Resta, R. (1999). Noncubic behavior of antiferromagnetic transition-metal monoxides with the rocksalt structure. *Phys. Rev. Lett.*, *82*, 430–433. DOI: 10.1103/PhysRevLett.82.430

50. Mironova-Ulmane, N., Kuzmin, A., Steins, I., Grabis, J., Sildos, I., & Pärs, M. (2007). Raman scattering in nanosized nickel oxide NiO. *J. Phys.: Conf. Ser.*, *93*, 012039. DOI: 10.1088/1742-6596/93/1/012039

51. Mironova-Ulmane, N., Kuzmin, A., Grabis, J., Sildos, I., Voronin, V., Berger, I., & Kazantsev, V. (2011). Structural and magnetic properties of nickel oxide nanopowders. *Solid State Phenomena*, *168–169*, 341–344. DOI: 10.4028/www.scientific.net/SSP.168-169.341

52. Gandhi, A. C., Pant, J., Pandit, S. D., Dalimbkar, S. K., Chan, T.-S., Cheng, C.-L., … & Wu, S. Y. (2013). Short-range magnon excitation in NiO nanoparticles. *J. Phys. Chem. C*, *117*, 18666–18674. DOI: 10.1021/jp4029479

53. Ravikumar, P., Kisan, B., & Perumal, A. (2015). Enhanced room temperature ferromagnetism in antiferromagnetic NiO nanoparticles. *AIP Adv.*, *5*, 087116. DOI: 10.1063/1.4928426

54. Mironova-Ulmane, N., Kuzmin, A., & Sildos, I. (2015). Template-based synthesis of nickel oxide. *IOP Conf. Ser.: Mater. Sci. Eng.*, *77*, 012025. DOI: 10.1088/1757-899X/77/1/012025

55. Mironova-Ulmane, N., Kuzmin, A., Sildos, I., & Pärs, M. (2011). Polarisation dependent Raman study of single-crystal nickel oxide. *Centr. Eur. J. Phys.*, *9*, 1096–1099. DOI: 10.2478/s11534-010-0130-9

56. Mironova-Ulmane, N., Kuzmin, A., Skvortsova, V., & Sildos, I. (2002). Exciton-magnon interactions in $Ni_cMg_{1-c}O$ single-crystals. *Phys. Solid State*, *44*, 1463–1467. DOI: 10.1134/1.1501338

57. Ishikawa, K., Fujima, N., & Komura, H. (1985). First-order Raman scattering in MgO micro-crystals. *J. Appl. Phys.*, *57*, 973–975. DOI: 10.1063/1.334701

58. Gouadec, G., & Colomban, P. (2007). Raman Spectroscopy of nanomaterials: How spectra relate to disorder, particle size and mechanical properties. *Progr. Crystal Growth Charact. Mater.*, *53*, 1–56. DOI: 10.1016/j.pcrysgrow.2007.01.001

59. Alders, D., Tjeng, L. H., Voogt, F. C., Hibma, T., Sawatzky, G. A., Chen, C. T., & Iacobucci, S. (1998). Temperature and thickness dependence of magnetic moments in NiO epitaxial films. *Phys. Rev. B*, *57*, 11623–11631. DOI: 10.1103/PhysRevB.57.11623

MAGNONU UN FONONU IEROSINĀŠANAS NANOIZMĒRA NIO

A N. Mironova-Ulmane, A. Kuzmins,
I. Sildos, L. Puust, J. Grabis

K o p s a v i l k u m s

Monokristāliskais, mikrokristāliskais un nanokristāliskais niķeļa oksīdi (NiO) tika pētīti, izmantojot Ramana spektroskopiju. Monokristāliskos NiO(100), NiO(110) un NiO(111) ir novērota jauna josla ap 200 cm^{-1} un TO-LO joslas sadalīšanās ap 350-650 cm^{-1}. Mikrokristāliska (1500 nm) un nanokristāliska (13-100 nm) NiO Ramana spektri ir līdzīgi monokristāliskam oksīdam. Tie visi satur divu magnonu joslu ap 1500 cm^{-1}, kas norāda, ka pie istabas temperatūras nanooksīdi atrodas antiferomagnētiskā stāvoklī. Nanokristāliskos NiO ir novērota arī jauna asa josla ap 500 cm^{-1}, kuras temperatūras atkarība norāda uz tās magnētisko izcelsmi, iespējams, saistītu ar fonona-magnonu ierosmi Briljuena zonas centrā.

23.11.2018.